AGU PUBLICATIONS

Geophysical Research Letters

RESEARCH LETTER
10.1002/2014GL062487

Key Points:
- Mercury's crustal thickness (35±18 km) much thinner than previously thought
- Mantle material excavated by major impact events may be observable on surface
- We estimate mantle heat production at 4.45 Ga to be in excess of 5.4×10^{-12} W/kg

Supporting Information:
- Readme
- Figures S1–S4 and Table S1

Correspondence to:
S. Padovan,
sebastiano.padovan@ucla.edu

Citation:
Padovan, S., M. A. Wieczorek, J.-L. Margot, N. Tosi, and S. C. Solomon (2015), Thickness of the crust of Mercury from geoid-to-topography ratios, *Geophys. Res. Lett.*, *42*, doi:10.1002/2014GL062487.

Received 10 NOV 2014
Accepted 3 JAN 2015
Accepted article online 8 JAN 2015

Thickness of the crust of Mercury from geoid-to-topography ratios

Sebastiano Padovan[1,2], Mark A. Wieczorek[2], Jean-Luc Margot[1,3], Nicola Tosi[4,5], and Sean C. Solomon[6,7]

[1]Department of Earth, Planetary, and Space Sciences, University of California, Los Angeles, California, USA, [2]Institut de Physique du Globe de Paris, Sorbonne Paris Cité, Université Paris Diderot, Paris, France, [3]Department of Physics and Astronomy, University of California, Los Angeles, California, USA, [4]Department of Astronomy and Astrophysics, Technische Universität Berlin, Berlin, Germany, [5]Department of Planetary Physics, German Aerospace Center, Berlin, Germany, [6]Lamont-Doherty Earth Observatory, Columbia University, Palisades, New York, USA, [7]Department of Terrestrial Magnetism, Carnegie Institution of Washington, Washington, District of Columbia, USA

Abstract To gain insight into the thickness of the crust of Mercury, we use gravity and topography data acquired by the MErcury Surface, Space ENvironment, GEochemistry, and Ranging spacecraft to calculate geoid-to-topography ratios over the northern hemisphere of the planet. For an Airy model for isostatic compensation of variations in topography, we infer an average crustal thickness of 35 ± 18 km. Combined with the value of the radius of the core of Mercury, this crustal thickness implies that Mercury had the highest efficiency of crustal production among the terrestrial planets. From the measured abundance of heat-producing elements on the surface, we calculate that the heat production in the mantle from long-lived radioactive elements at 4.45 Ga was greater than 5.4×10^{-12} W/kg. By analogy with the Moon, the relatively thin crust of Mercury allows for the possibility that major impact events, such as the one that formed the Caloris basin, excavated material from Mercury's mantle.

1. Introduction

Planetary crusts are formed and shaped during major igneous events such as magma ocean solidification and large-scale volcanism. These processes affect the thermochemical evolution of the interior through a number of processes [e.g., *Elkins-Tanton*, 2012], including the partitioning of incompatible heat-producing elements, which during episodes of partial melting concentrate into the melt and accumulate in the crust; the modification of the bulk volatile content, given that volatile elements in near-surface magmas tend to escape to the atmosphere; and the modification of the internal temperature profile by the transport of hot material from the deep interior to shallow depths. Characterization of the crust thus provides information on the origin, differentiation, and subsequent geologic evolution of a planetary body. For Mercury, in particular, the crust may hold clues to the still poorly understood processes of formation of this planet.

There have been a number of attempts to constrain the thickness of the crust of Mercury. *Anderson et al.* [1996] compared the magnitude of the spherical harmonic second-degree sectorial gravitational coefficient C_{22} obtained by radio tracking of the Mariner 10 spacecraft with the value inferred from the equatorial ellipticity in elevation, measured with Earth-based radar observations, and assumed that the topography of Mercury at degree 2 is compensated. Under the assumption of Airy isostasy, they inferred that the thickness of the crust lies in the range 100 to 300 km.

Lobate scarps observed on the surface of Mercury are interpreted to be the surface manifestations of large thrust faults [e.g., *Strom et al.*, 1975]. Topographic profiles across thrust faults constrain the deepest extent of faulting to be 35 to 40 km [*Watters et al.*, 2002]. By analogy with thermal limits to brittle behavior on Earth, the depth of faulting provides a constraint on the subsurface thermal structure, and therefore heat flux, at the time of fault formation [*Nimmo*, 2002; *Watters et al.*, 2002]. Combining this information with a model for the viscous relaxation of topography and its compensation at the crust-mantle boundary constrains the crustal thickness to be < 200 km [*Nimmo*, 2002]. This value is an upper bound since it was obtained without taking into account the secular cooling of the planet, which would increase the estimate of early heat flux and thereby reduce the maximum thickness of the crust [*Nimmo*, 2002].

Nimmo and Watters [2004] inferred an upper limit of 140 km on the crustal thickness by combining the inferred maximum depth of faulting with the requirement that the base of the crust does not remelt. The latter requirement was enforced by using a reference melting temperature for crustal materials of 1800 K. For a more likely value of 1500 K, the upper bound on the crustal thickness would be about 90 km [*Nimmo and Watters*, 2004].

A joint analysis of gravity and topography data can be used to characterize the subsurface structure of rocky planets [e.g., *Wieczorek*, 2007]. *Smith et al.* [2012] combined the gravity and topography of Mercury measured by the MErcury Surface, Space ENvironment, GEochemistry, and Ranging (MESSENGER) spacecraft to produce a map of crustal thickness for the northern hemisphere. This map was obtained with an assumed value for the mean crustal thickness, and the uncertainty in this mean value represents the largest uncertainty in the model [*Smith et al.*, 2012]. In this work we calculate spatially localized geoid-to-topography ratios (GTRs) over the surface of Mercury and interpret these ratios with the method of spectrally weighted admittances [*Wieczorek and Phillips*, 1997]. This method has been previously applied to infer the thickness of the crust of the Moon [*Wieczorek and Phillips*, 1997; *Wieczorek et al.*, 2006], Mars [*Wieczorek and Zuber*, 2004], and Venus [*James et al.*, 2013].

2. Data and Methods

We calculated the geoid of Mercury from the spherical harmonic model HgM005 for the gravitational potential, a model complete to degree and order 50 [*Mazarico et al.*, 2015]. The shape of the planet was obtained from a spherical harmonic model of the topography [*Neumann*, 2014]. Since the analysis used here is based on the relation between gravity and topography, the topographic expansion was truncated at the same degree as the geoid.

We computed the value of the geoid N and topography h over a global grid with a constant spacing of about $1.5° \times 1.5°$, resulting in almost 20,300 grid points. Both the geoid heights and surface topography were referenced to the same radius, which we chose to be the mean planetary radius $R = 2440$ km, and the geoid was calculated from Brun's equation, which is a first-order approximation that gives rise to an error of less than 1 m for Mercury [*Wieczorek*, 2007, 2015]. The GTRs for each grid point were computed from regressions of geoid and topography data within spherical caps of radius r according to the equation

$$N = \mathrm{GTR}\, h + b_0, \tag{1}$$

where b_0 is a constant. Our results are insensitive to variations in cap radius from $r = 1250$ km to $r = 2000$ km, though the uncertainty in the GTR from the regression decreases with increasing cap dimension. From the trade-off between spatial resolution and GTR uncertainty, $r = 2000$ km is our preferred choice for the radius of the spherical cap. If the geoid signals were due only to lateral variations in the thickness of a crust of constant density, the b_0 term in equation (1) would be zero if all elevations were referenced to the mean planetary radius. A nonzero b_0 is included to account for possible contributions from regional variations in crustal density, density anomalies in the mantle, or spherical harmonic degree 1 topography (which does not have an expression in the geoid in coordinates for which the origin is at the center of mass). With different statistical tests (adjusted coefficient of determination, F-test, and Akaike information criterion [see, e.g., *Feigelson and Babu*, 2012]) we established that a two-parameter model (GTR and b_0) is to be preferred over a one-parameter model with $b_0 = 0$.

The calculated GTR is interpreted in the framework of spectrally weighted admittances [*Wieczorek and Phillips*, 1997]. If the GTR is spatially stationary over the analyzed region, it can be expressed as

$$\mathrm{GTR} = \sum_{l_{min}}^{l_{max}} W_l Z_l, \tag{2}$$

where W_l is a weighting function that depends on the topographic power spectrum and is given by

$$W_l = \frac{S_{hh}(l)}{\sum_{l_{min}}^{l_{max}} S_{hh}(l)}, \tag{3}$$

and where S_{hh} is the topographic power at degree l. Z_l is a degree-dependent admittance function that relates the harmonic coefficients of the geoid to those of the topography. In the summations

of equations (2) and (3), the lower limit l_{min} is chosen on the basis of consistency with the assumed compensation mechanism (section 3). The upper limit l_{max} is dictated by the quality of the measured fields, and it is set to 50, the nominal resolution of the gravitational field. Note, however, that since the power in planetary topography decreases with increasing degree [*Bills and Lemoine*, 1995], the function W_l assigns more weight to the lowest degrees and the choice of l_{max} is not crucial. We confirmed this inference by finding no important difference between results obtained with l_{max} equal to 50 and those with l_{max} equal to 20.

The analytical expression for Z_l in equation (2) depends on the assumed compensation model. The differentiated nature of terrestrial planets indicates that early in their evolution the temperature of the interior was sufficiently high for the silicates to be separated from a metallic component that settled to the core. The temperature of the early crust would have been close to the solidus, if the crust formed through the solidification of a magma ocean [*Elkins-Tanton*, 2012] or if it was later modified as a result of giant impacts [e.g., *Benz et al.*, 1988]. Because high temperatures decrease the elastic strength of the lithosphere [e.g., *Kampfmann and Berckhemer*, 1985], long-wavelength topographic loads are not likely to be supported by lithospheric strength [*Turcotte et al.*, 1981]. Therefore, we assume that a local compensation mechanism, Airy isostasy, is the principal mechanism of support of the long-wavelength variations in the thickness of the crust, which probably formed early in planetary evolution. In the Airy isostatic compensation model, the excess of surface relief is balanced by a crustal root. Though the use of a geoid-to-topography ratio cannot prove that Airy isostasy has been achieved, we note that the same assumption has been used in studies of the ancient crusts of other terrestrial bodies [*Wieczorek and Phillips*, 1997; *Wieczorek and Zuber*, 2004; *James et al.*, 2013]. Regions on Mercury where this assumption might be invalid are excluded from the analysis (section 3). For Airy isostatic compensation, the thickness of the crust H under a surface with topography h is [e.g., *Lambeck*, 1988]

$$H = H_0 + h\left[1 + \frac{\rho_c}{\rho_m - \rho_c}\left(\frac{R}{R - H_0}\right)^2\right], \tag{4}$$

where H_0 is the zero-elevation crustal thickness, the radius of the planet is R, and ρ_c and ρ_m are the densities of the crust and the mantle, respectively, each assumed to be uniform. The corresponding admittance function Z_l is given by the expression [e.g., *Lambeck*, 1988]

$$Z_l = \frac{3}{2l+1}\frac{\rho_c}{\rho}\left[1 - \left(\frac{R-H}{R}\right)^l\right], \tag{5}$$

with ρ the mean density of the planet. Equations (2) and (5) show that, under the assumption of a given compensation mechanism and for a given choice of the crustal density ρ_c, measurements of the GTR can be inverted for the crustal thickness H.

By calculating the normative mineralogy from the elemental abundance measurements of *Weider et al.* [2012], we estimated the grain density of the northern volcanic plains material and the material in Mercury's heavily cratered terrain and intercrater plains to be 3014 kg/m^3 and 3082 kg/m^3, respectively. Our calculated mineralogies for these two units compare favorably with those from the petrological modeling of *Stockstill-Cahill et al.* [2012]. Allowing for a porosity of up to 12% that might extend down to the mantle, as has been demonstrated for the Moon [*Wieczorek et al.*, 2013], we consider a conservative range in crustal densities of 2700–3100 kg/m^3. For comparison, *Anderson et al.* [1996] assumed a crustal density ρ_c of 3000 kg/m^3, *Nimmo* [2002] and *Nimmo and Watters* [2004] adopted $\rho_c = 2800$ kg/m^3, and *Smith et al.* [2012] assumed a value for ρ_c of 3100 kg/m^3. Our range in crustal density, derived from data returned by MESSENGER and the possibility of a Moon-like porosity for the crust, encompasses all of these values.

3. Results

The orbit of MESSENGER is highly eccentric, and the periapsis latitude has varied between 60°N and 85°N. The reconstructed gravitational field in the southern hemisphere, where MESSENGER is at high altitudes, is thus of low resolution. This result is exemplified by the degree strength of the gravitational field, which describes the location-dependent harmonic degree at which the signal-to-noise ratio of the data is equal to one [*Konopliv et al.*, 1999]. A map of the degree strength for Mercury shows that the degree strength increases as a function of latitude, from about 15 on the equator to 36 near the north pole

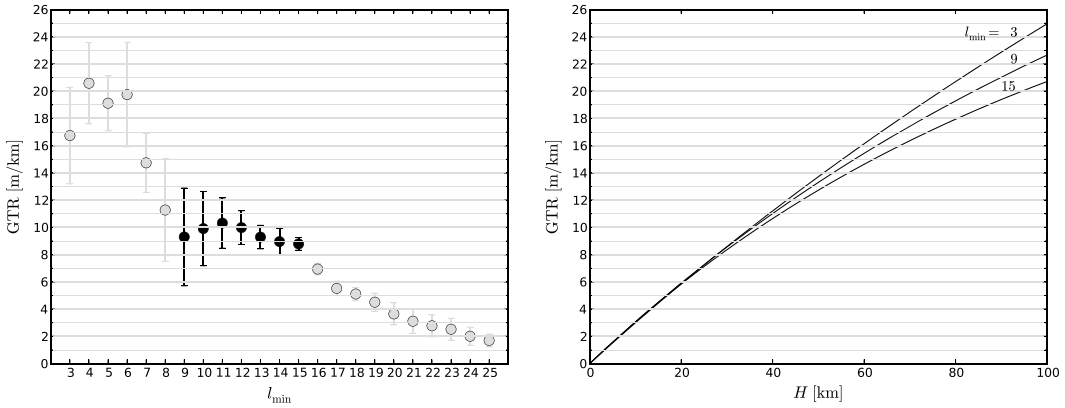

Figure 1. (left) Geoid-to-topography ratio as a function of the high-pass filter cutoff l_{min} applied to the geoid and topography data. Values are obtained by regressing the two data sets within spherical caps of 2000 km radius and including only those regions compatible with the assumption of Airy isostasy. The signal interpreted as due to Airy-compensated crust is shown in black. (right) Theoretical relation between GTR and crustal thickness for a crustal density of 2900 kg/m^3 and for different values of the high-pass filter cutoff l_{min}.

[*Mazarico et al.*, 2015]. Over the southern hemisphere there is little altimetry data, so in our analysis we considered data only from Mercury's northern hemisphere.

Large areas on the surface of Mercury are covered by smooth plains, the majority of which are inferred to be volcanic in origin [*Denevi et al.*, 2013]. If the lavas that formed these plains erupted when the lithosphere was sufficiently thick to support surface loads, these regions might not satisfy our assumption of Airy isostasy. Moreover, a number of large impact craters and basins have been identified on Mercury [*Fassett et al.*, 2012], and as is the case on the Moon and Mars, these features might depart from local isostasy [e.g., *Melosh et al.*, 2013]. We excluded from the analysis all data within the rims of impact basins having diameters greater than 490 km and all regions covered by mapped expanses of smooth plains, as illustrated in Figure S1 in the supporting information. We tested that a smaller cutoff diameter for large basins did not modify the derived crustal thickness.

In the calculation of the value of the GTR within a given spherical cap, all points on smooth plains, inside large craters, or located in the southern hemisphere were discarded. If the fraction of discarded points within the cap exceeded 50%, the GTR value for that cap was discarded. (The error in the GTR value for each cap is typically smaller than 10%.) The calculated GTR as a function of the high-pass filter l_{min} for remaining areas on Mercury's surface is plotted in Figure 1; the error shown for each degree corresponds to the standard deviation of the population of GTRs obtained from the analysis. For $l_{min} = 2$ the GTR is about 38 m/km. This value is much larger than the GTRs for $l_{min} > 2$, and it is not included in Figure 1 for clarity. For l_{min} from 3 to 6 the value of the GTR is also high, with values between 16 and 21 m/km. The GTR decreases for l_{min} from 7 to 8, and then for greater values of l_{min}, the GTR is relatively constant at a value of about 9 m/km. The GTRs steadily decrease with increasing l_{min} beyond 16, a figure that corresponds approximately to the degree strength of the gravitational field at the equator. Therefore, we interpret this decrease to be a reflection of the decrease in the quality and resolution of the gravity field with increasing degree above this cutoff.

We also calculated the GTR as a function of the high-pass filter cutoff l_{min} for regions initially excluded because of a possible incompatibility with the assumption of Airy isostasy (i.e., smooth plains and large craters in the northern hemisphere, Figure S1). In contrast with Figure 1, the near-constant value of GTR between degrees 9 and 15 is absent, whereas values of GTR for $l_{min} < 9$ are compatible with those in Figure 1 (see Figure S2). This difference in behavior for l_{min} from 9 to 15 justifies our assumption that the compensation state of basins and smooth plains differs from that for the surrounding heavily cratered terrain and intercrater plains. Under Airy isostasy, the predicted GTRs should be nearly uniform and independent of the value of l_{min}. Therefore, we regard the near constancy of GTR values in Figure 1 between $l_{min} = 9$ and 15 as a signal of Airy isostasy for those length scales.

A possible interpretation of the variation of GTR with $l_{min} < 9$ is that the ratios at these long wavelengths include contributions from Mercury's mantle. Such variations could be the result of mantle convection, lateral variations in mantle composition [*Charlier et al.*, 2013], or lateral variations in temperature. To further investigate this possibility, we explore the behavior of the parameter b_0 from equation (1). For increasing l_{min} the residual signal in b_0 is concentrated in the Caloris basin and the northern smooth plains, locations where non-Airy isostatic signals are expected (Figure S3). In contrast, for those regions compatible with the assumption of Airy isostasy, b_0 is found to decrease with increasing l_{min}, and for l_{min} greater than about 7–9, this value is close to zero. This outcome further supports our interpretation that the GTRs for $l_{min} \geq 9$ are a result of Airy isostasy.

Although the mantle of Mercury is likely to be in a conductive state at present, a currently convecting mantle cannot be ruled out [*Michel et al.*, 2013; *Tosi et al.*, 2013]. To test whether the GTR signal for $l_{min} < 9$ might include a contribution from convection in the mantle, we compared the power spectra of the observed topography and geoid with those obtained from a representative simulation of the thermochemical evolution of Mercury in which the mantle is still convecting today. These convection simulations were performed in a three-dimensional spherical shell with the code Gaia [*Hüttig and Stemmer*, 2008] following the methods of *Tosi et al.* [2013] but constrained by recently revised estimates of the global contraction of the planet (at least 5.8 km) since the end of the late heavy bombardment of the inner solar system [*Byrne et al.*, 2014]. Calculation of the geoid and dynamic topography with Gaia has been validated against well-established semianalytical solutions [*Hüttig et al.*, 2013].

The geoid and topography spectra from the simulations (Figure S4) are orders of magnitude smaller than the observed spectra, indicating that even if the mantle were still convecting, this signal should not bias the observed GTR. We note that this result contrasts with previous convection simulations of *Redmond and King* [2007], who obtained variations in the geoid of tens of meters. *Michel et al.* [2013] showed that the current mode of heat transport in the mantle of Mercury depends on the thickness of the planet's silicate shell, with strong convection favored for greater values of the depth to the core-mantle boundary. *Redmond and King* [2007], using pre-MESSENGER information, assumed a value of 600 km for the thickness of the mantle, in contrast to the value of ~400 km implied by MESSENGER observations [*Hauck et al.*, 2013; *Rivoldini and Van Hoolst*, 2013]. This, along with their use of a Cartesian domain for their simulations, is the likely explanation for the difference between their results and the simulations presented here.

In addition to a signal derived from Airy isostasy, there may also be a contribution to the GTR at long wavelength from lateral variations in temperature within Mercury. Mercury has a very low obliquity [*Margot et al.*, 2012] and a highly eccentric orbit [*Correia and Laskar*, 2004] and is locked in a 3:2 spin-orbit resonance [*Colombo*, 1965; *Pettengill and Dyce*, 1965]. As first pointed out by *Soter and Ulrichs* [1967], the combination of these characteristics results in two equatorial locations that are subsolar at perihelion (Mercury's "hot poles" at longitudes 0° and 180°E), and two equatorial locations that are subsolar at aphelion (Mercury's "warm poles" at longitudes 90°E and 270°E). The highest insolation occurs at the hot poles and results in an average temperature difference between hot and warm poles of about 130 K [*Soter and Ulrichs*, 1967]. Mercury's "cold poles" are at the north and south rotational poles. *Phillips et al.* [2014] showed that the degree 2 gravity and topography signal is likely dominated by thermal effects resulting from subsurface temperature anomalies induced by the surface temperature pattern. A spherical harmonic expansion of the surface temperature shows that the greatest power is concentrated in degrees 2 (~90%) and 4 (~10%). It is thus probable that both the degrees 2 and 4 signals in the GTR are affected by thermal anomalies associated with variations in surface insolation, so these degrees should be excluded from the GTR analysis. For all of the above reasons, we restrict the remaining discussion to GTR values obtained with l_{min} in the range 9 to 15 (black points in Figure 1).

The theoretical relation between GTR and crustal thickness, obtained from equations (2) and (5) with a crustal density $\rho_c = 2900$ kg/m^3, is shown in Figure 1 (right). From this relationship, the crustal thickness corresponding to each calculated GTR was estimated, and since the average elevation of each analysis region is not always equal to zero, we estimated the corresponding crustal thickness at zero elevation under the assumption of Airy isostasy from equation (4). For a mantle density $\rho_m = 3300$ kg/m^3, a histogram of the inferred zero-elevation crustal thickness H_0 is shown in Figure 2 for l_{min} from 9 to 15. As for the GTR, the error shown for each degree is taken to equal the standard deviation of the population of H_0 values obtained from the GTR values. The average value of H_0 is approximately independent of the value of the

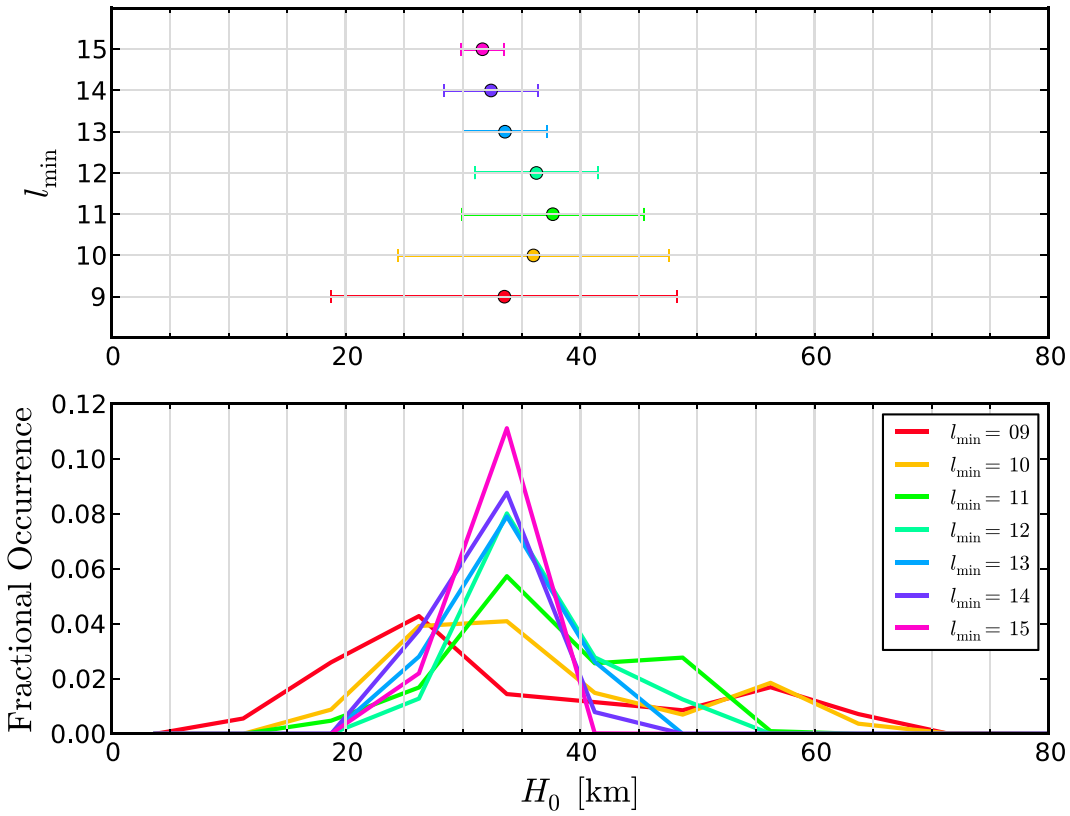

Figure 2. Average crustal thickness at zero-elevation H_0 of Mercury obtained from the calculated GTR (black symbols in Figure 1 (left)) for a crustal density of 2900 kg/m^3 and a mantle density of 3300 kg/m^3. (top) Average and standard deviation of H_0 as functions of the high-pass filter cutoff $l_{\min}$. (bottom) Histograms of the calculated crustal thickness H_0.

high-pass filter cutoff, and the uncertainty decreases somewhat with increasing $l_{\min}$. A conservative estimate for the thickness of the crust of Mercury is obtained by combining the results for $l_{\min} = 9$, which has the largest uncertainty, with our calculated bounds on the crustal density of 2700 and 3100 kg/m^3. For our best fit crustal thickness, we give the average obtained from the upper and lower bounds on crustal density for $l_{\min} = 9$, and for uncertainty we give the maximum of the corresponding one-standard-deviation limits. On this basis, we obtain an average crustal thickness of the planet of $H_0 = 35 \pm 18$ km.

4. Discussion and Implications

Our estimate for the average crustal thickness of Mercury is considerably less than previously reported values. The value obtained by *Anderson et al.* [1996] is seemingly in contradiction with ours, and we reevaluate their estimate with updated MESSENGER-derived values of the gravitational and topographic C_{22} terms [*Smith et al.*, 2012; *Zuber et al.*, 2012]. Using the same approach as *Anderson et al.* [1996], we revise their estimate downward from 200 to 171 km. If we were to have inferred the crustal thickness from our GTR analysis by setting the high-pass filter cutoff $l_{\min} = 2$, we would have obtained a similarly high crustal thickness $H_0 = 160 \pm 32$ km. With a silicate shell no more than ~400 km thick, however, it is highly improbable that the crustal thickness could be so large. The degree 2 gravity and topography are thus likely to reflect processes other than local Airy isostasy. Other studies provided only upper bounds on the crustal thickness [*Nimmo*, 2002; *Nimmo and Watters*, 2004], and they are consistent with our value of 35 ± 18 km.

The crust of Mercury has a thickness comparable to the thickness of the crust of the Moon ($H = 38.5 \pm 4.5$ km [*Wieczorek et al.*, 2013]), Venus ($H = 16.5 \pm 8.5$ km [*James et al.*, 2013]), and Mars ($H = 57 \pm 24$ km [*Wieczorek and Zuber*, 2004]), as well as that of the continental crust on Earth (H ~35 km [e.g., *Turcotte and Schubert*, 2002]). The relative size of the radius of the core of Mercury (~82.5% of the radius of the planet, or 2014 km) [*Hauck et al.*, 2013; *Rivoldini and Van Hoolst*, 2013] is the largest among the terrestrial planets. As a result, the volume of the crust accounts for about 10% of the total volume of silicate materials in the planet. This

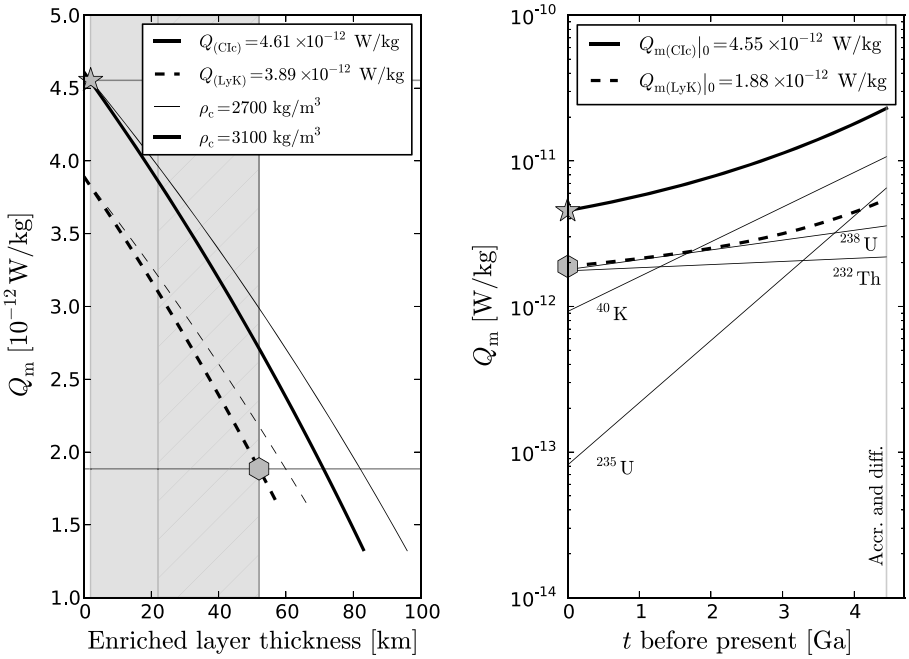

Figure 3. Heat production in the mantle Q_m from radioactive decay of K, Th, and U. (left) Current heat production as a function of the thickness of an enriched surficial layer for two crustal densities (indicated by the line thickness) and two bulk silicate abundances derived from the primitive Earth mantle model of *Lyubetskaya and Korenaga* [2007] (LyK, dashed lines) and the CI chondrite model of *McDonough and Sun* [1995] (CIc, solid lines). The shaded area spans the interval 2–53 km; the lower limit corresponds to the estimated thickness of the northern plains deposits [*Head et al.*, 2011] and the higher limit to the maximum value of the crustal thickness as inferred from the GTR analysis (hashed area). The minimum and maximum values of Q_m are indicated by the hexagon and the star, respectively. (right) Mantle heat production as a function of time for the minimum and maximum values obtained from the left panel. The bold lines show the total heat production for the CIc model (solid) and the LyK model (dashed). For the CIc model the contributions of individual isotopes are also shown. The vertical line indicates the approximate time of completion of accretion and differentiation of the planet (4.45 Ga).

value is the highest among the terrestrial planets and implies that Mercury had the highest efficiency of crustal production. (For comparison the fraction of silicates in the crust is about 7% for the Moon and 5% for Mars, and for Venus the fraction is probably similar to Earth's value, i.e., less than 2%.) If the thickness of the northern plains (~2 km) [*Head et al.*, 2011] is representative of the contribution to the crust produced by the most recent widespread episodes of partial melting of the mantle, then a large fraction of Mercury's crust was produced early in its history.

Modeling the thermochemical evolution of the terrestrial planets requires knowledge of the amount of radioactive elements in both the mantle and the crust [e.g., *Schubert et al.*, 2001], which for Mercury can be evaluated with our estimate of crustal thickness. The abundances on the surface of Mercury of the heat-producing elements K, Th, and U have been measured with the Gamma-Ray Spectrometer on MESSENGER [*Peplowski et al.*, 2011, 2012]. If the abundances of these elements are uniform within a surficial enriched layer, then the thickness of such a layer can be inferred to lie between about 2 km, the approximate thickness of the northern plains deposits [*Head et al.*, 2011], and 53 km, our upper bound on the crustal thickness. The nonenriched part of the crust is assumed to have the same abundances of incompatible elements as the mantle. With assumed values of bulk abundances of heat-producing elements in the silicate part of the planet, it is then possible, by mass balance, to estimate the current abundances of each of these elements in the mantle and their contribution to heat production as a function of time. Because the bulk silicate composition of Mercury is not known, we use two end-member models: the primitive Earth mantle model of *Lyubetskaya and Korenaga* [2007] and the CI chondrite model of *McDonough and Sun* [1995]. For the mean density of the silicate shell of Mercury we use the value 3380 kg m^{-3} [*Hauck et al.*, 2013].

The current mantle heat production Q_m as a function of the thickness of the enriched layer is shown in Figure 3 (left). The curves correspond to different crustal densities and bulk abundance of heat-producing

elements. Each curve is interrupted at the point at which the mass balance calculation returns a zero abundance for one of the three heat-producing elements. This set of calculations allows maximum and minimum values for Q_m at present to be determined, respectively, 4.55×10^{-12} and 1.88×10^{-12} W/kg (the abundances of each heat-producing element are reported in Table S1). From these two values, the mantle heat production as a function of time can then be calculated (Figure 3, right). A lower bound on the mantle heat production at a time following accretion and differentiation (~4.45 Ga, a value obtained by subtracting 100 My, a reference interval of time for the accretion and differentiation of terrestrial planets, e.g., *Jacobson et al.* [2014], from the time of the formation of the solar system, ~4.55 Ga [*Bouvier and Wadhwa*, 2010]) is obtained under the assumption that the concentration of radioactive elements into the crust dates back to the earliest history of Mercury. Under such an assumption the mantle heat production would have been in the range 5.4×10^{-12} to 2.3×10^{-11} W/kg. This interval is consistent with, but slightly more restrictive than, the lower bound on initial mantle heat production of 3×10^{-12} W/kg adopted by *Redmond and King* [2007], and it partially overlaps the lower range of initial mantle heat production explored by *Michel et al.* [2013] (from 1×10^{-11} to 1.25×10^{-10} W/kg). Such a value for mantle heat production corresponds to a crustal enrichment factor between 3.4 and 14.5; for comparison, the range for this factor assumed by *Tosi et al.* [2013] was between 2 and 10.

Models for the formation of major impact basins on the Moon suggest that some may have excavated mantle material at the time of impact and left such material exposed on the modern lunar surface [*Miljković et al.*, 2015]. The similarly thin crust of Mercury therefore opens the possibility of excavation of mantle material during the formation of the largest impact basins, such as Caloris. The identification and characterization of mantle material would provide valuable information on the composition of the bulk silicate portion of the planet, which in turn would be informative of the planet's formation [e.g., *Taylor and Scott*, 2005] and interior structure [*Hauck et al.*, 2013; *Rivoldini and Van Hoolst*, 2013; *Padovan et al.*, 2014].

5. Conclusions

With gravity and topography data acquired by the MESSENGER spacecraft we have calculated geoid-to-topography ratios (GTRs) over the northern hemisphere of Mercury. Excluding the longest wavelengths, which are likely to be sensitive to long-wavelength variations in interior thermal structure associated with Mercury's low obliquity and 3:2 spin-orbit resonance, as well as possible lateral variations in the composition of Mercury's mantle, we assume that Airy isostasy is responsible for the remaining signal. This analysis implies that the average crustal thickness of Mercury is 35 ± 18 km.

This new mean value is substantially smaller than earlier estimates [*Anderson et al.*, 1996; *Nimmo*, 2002; *Nimmo and Watters*, 2004] and is broadly similar to the thickness of the crust of the other terrestrial planets and the Moon. Given the large core size of Mercury, the crust comprises about 10% of the silicate volume, a value that is the largest among the terrestrial planets and points to a high efficiency of crustal production. With such a thin crust, it is possible that the formation of the major impact basins may have excavated mantle material that is currently exposed on the surface. A search for such exposed mantle material is warranted in observations acquired by MESSENGER and future spacecraft missions at Mercury.

By combining our crustal thickness determination with the abundances of heat-producing elements on the surface of Mercury measured by MESSENGER [*Peplowski et al.*, 2011, 2012], we constrain the amount of heat produced in the mantle over time. Our results are broadly consistent with assumptions made in previous studies of the thermal evolution of the mantle of Mercury [*Redmond and King*, 2007; *Michel et al.*, 2013; *Tosi et al.*, 2013] and can inform future models of the thermochemical evolution of the planet.

Acknowledgments

We thank all the individuals who designed and operate the MESSENGER spacecraft. We are grateful to Brett Denevi for providing the locations of mapped smooth plains. The spherical harmonic expansions for the gravitational field and topography of Mercury are available from the Planetary Data System (|http://tinyurl.com/o8u98bc|). Part of the calculations used the freely available software SHTOOLS [*Wieczorek*, 2014], and the figures were created with the free software described by *Wessel and Smith* [1991] and *Hunter* [2007]. This work was conducted while S.P. was visiting M.A.W. with the support of a Chateaubriand Fellowship. S.P. and J.-L.M. were partially supported by MESSENGER Participating Scientist Program grant NNX09AR45G and by the UCLA Division of Physical Sciences. N.T. was partially supported by the DFG (project T0704/1-1) and by the Helmholtz Gemeinschaft (project VH-NG-1017). Computational time for the convection simulations was provided by the HLRN (project bep0041). The MESSENGER project is supported by the NASA Discovery Program under contracts NAS5-97271 to The Johns Hopkins University Applied Physics Laboratory and NASW-00002 to the Carnegie Institution of Washington.

The Editor thanks two anonymous reviewers for their assistance in evaluating this paper.

References

Anderson, J. D., R. F. Jurgens, E. L. Lau, M. A. Slade III, and G. Schubert (1996), Shape and orientation of Mercury from radar ranging data, *Icarus*, *124*, 690–697, doi:10.1006/icar.1996.0242.

Benz, W., W. L. Slattery, and A. G. W. Cameron (1988), Collisional stripping of Mercury's mantle, *Icarus*, *74*, 516–528, doi:10.1016/0019-1035(88)90118-2.

Bills, B. G., and F. G. Lemoine (1995), Gravitational and topographic isotropy of the Earth, Moon, Mars, and Venus, *J. Geophys. Res.*, *100*, 26,275–26,296, doi:10.1029/95JE02982.

Bouvier, A., and M. Wadhwa (2010), The age of the solar system redefined by the oldest Pb-Pb age of a meteoritic inclusion, *Nat. Geosci.*, *3*, 637–641, doi:10.1038/ngeo941.

Byrne, P. K., C. Klimczak, A. M. C. Şengör, S. C. Solomon, T. R. Watters, and S. A. Hauck II (2014), Mercury's global contraction much greater than earlier estimates, *Nat. Geosci.*, *7*, 301–307, doi:10.1038/ngeo2097.

Charlier, B., T. L. Grove, and M. T. Zuber (2013), Phase equilibria of ultramafic compositions on Mercury and the origin of the compositional dichotomy, *Earth Planet. Sci. Lett.*, *363*, 50–60, doi:10.1016/j.epsl.2012.12.021.
Colombo, G. (1965), Rotational period of the planet Mercury, *Nature*, *208*, 575, doi:10.1038/208575a0.
Correia, A. C. M., and J. Laskar (2004), Mercury's capture into the 3/2 spin-orbit resonance as a result of its chaotic dynamics, *Nature*, *429*, 848–850, doi:10.1038/nature02609.
Denevi, B. W., et al. (2013), The distribution and origin of smooth plains on Mercury, *J. Geophys. Res. Planets*, *118*, 891–907, doi:10.1002/jgre.20075.
Elkins-Tanton, L. T. (2012), Magma oceans in the inner solar system, *Annu. Rev. Earth Planet. Sci.*, *40*, 113–139, doi:10.1146/annurev-earth-042711-105503.
Fassett, C. I., et al. (2012), Large impact basins on Mercury: Global distribution, characteristics, and modification history from MESSENGER orbital data, *J. Geophys. Res.*, *117*, E00L08, doi:10.1029/2012JE004154.
Feigelson, E., and G. Babu (2012), *Modern Statistical Methods for Astronomy: With R Applications*, Cambridge Univ. Press, Cambridge, U. K.
Hauck, S. A., II et al. (2013), The curious case of Mercury's internal structure, *J. Geophys. Res. Planets*, *118*, 1204–1220, doi:10.1002/jgre.20091.
Head, J. W., et al. (2011), Flood volcanism in the northern high latitudes of Mercury revealed by MESSENGER, *Science*, *333*, 1853–1856, doi:10.1126/science.1211997.
Hunter, J. D. (2007), Matplotlib: A 2D graphics environment, *Comput. Sci. Eng.*, *9*, 90–95.
Hüttig, C., and K. Stemmer (2008), Finite volume discretization for dynamic viscosities on Voronoi grids, *Phys. Earth Planet. Inter.*, *171*, 137–146, doi:10.1016/j.pepi.2008.07.007.
Hüttig, C., N. Tosi, and W. B. Moore (2013), An improved formulation of the incompressible Navier-Stokes equations with variable viscosity, *Phys. Earth Planet. Inter.*, *220*, 11–18, doi:10.1016/j.pepi.2013.04.002.
Jacobson, S. A., A. Morbidelli, S. N. Raymond, D. P. O'Brien, K. J. Walsh, and D. C. Rubie (2014), Highly siderophile elements in Earth's mantle as a clock for the Moon-forming impact, *Nature*, *508*, 84–87, doi:10.1038/nature13172.
James, P. B., M. T. Zuber, and R. J. Phillips (2013), Crustal thickness and support of topography on Venus, *J. Geophys. Res. Planets*, *118*, 859–875, doi:10.1029/2012JE004237.
Kampfmann, W., and H. Berckhemer (1985), High temperature experiments on the elastic and anelastic behaviour of magmatic rocks, *Phys. Earth Planet. Inter.*, *40*, 223–247, doi:10.1016/0031-9201(85)90132-3.
Konopliv, A. S., W. B. Banerdt, and W. L. Sjogren (1999), Venus gravity: 180th degree and order model, *Icarus*, *139*, 3–18.
Lambeck, K. (1988), *Geophysical Geodesy: The Slow Deformations of the Earth*, Clarendon Press, Oxford Science Publications, U. K.
Lyubetskaya, T., and J. Korenaga (2007), Chemical composition of Earth's primitive mantle and its variance: 1. Method and results, *J. Geophys. Res.*, *112*, B03211, doi:10.1029/2005JB004223.
Margot, J.-L., S. J. Peale, S. C. Solomon, S. A. Hauck II, F. D. Ghigo, R. F. Jurgens, M. Yseboodt, J. D. Giorgini, S. Padovan, and D. B. Campbell (2012), Mercury's moment of inertia from spin and gravity data, *J. Geophys. Res.*, *117*, E00L09, doi:10.1029/2012JE004161.
Mazarico, E., A. Genova, S. J. Goossens, F. G. Lemoine, G. A. Neumann, M. T. Zuber, D. E. Smith, and S. C. Solomon (2015), The gravity field, orientation, and ephemeris of Mercury from MESSENGER observations after three years in orbit, *J. Geophys. Res. Planets*, *119*, 2417–2436, doi:10.1002/2014JE004675.
McDonough, W. F., and S. S. Sun (1995), The composition of the Earth, *Chem. Geol.*, *120*, 223–253, doi:10.1016/0009-2541(94)00140-4.
Melosh, H. J., A. M. Freed, B. C. Johnson, D. M. Blair, J. C. Andrews-Hanna, G. A. Neumann, R. J. Phillips, D. E. Smith, S. C. Solomon, M. A. Wieczorek, and M. T. Zuber (2013), The origin of lunar mascon basins, *Science*, *340*, 1552–1555, doi:10.1126/science.1235768.
Michel, N. C., S. A. Hauck II, S. C. Solomon, R. J. Phillips, J. H. Roberts, and M. T. Zuber (2013), Thermal evolution of Mercury as constrained by MESSENGER observations, *J. Geophys. Res. Planets*, *118*, 1033–1044, doi:10.1002/jgre.20049.
Miljković, K., M. A. Wieczorek, G. S. Collins, S. C. Solomon, D. E. Smith, and M. T. Zuber (2015), Excavation of the lunar mantle by basin-forming impact events on the Moon, *Earth Planet. Sci. Lett.*, *409*, 243–251, doi:10.1016/j.epsl.2014.10.041.
Neumann, G. A. (2014), Spherical harmonic expansion for the topography of Mercury, *GTMES_120V02_SHA*, NASA Planetary Data System. [Available at http://pds-geosciences.wustl.edu/messenger/mess-h-rss_mla-5-sdp-v1/messrs_1001/data/.]
Nimmo, F. (2002), Constraining the crustal thickness on Mercury from viscous topographic relaxation, *Geophys. Res. Lett.*, *29*, 1063, doi:10.1029/2001GL013883.
Nimmo, F., and T. R. Watters (2004), Depth of faulting on Mercury: Implications for heat flux and crustal and effective elastic thickness, *Geophys. Res. Lett.*, *31*, L02701, doi:10.1029/2003GL018847.
Padovan, S., J.-L. Margot, S. A. Hauck II, W. B. Moore, and S. C. Solomon (2014), The tides of Mercury and possible implications for its interior structure, *J. Geophys. Res. Planets*, *119*, 850–866, doi:10.1002/2013JE004459.
Peplowski, P. N., et al. (2011), Radioactive elements on Mercury's surface from MESSENGER: Implications for the planet's formation and evolution, *Science*, *333*, 1850–1852, doi:10.1126/science.1211576.
Peplowski, P. N., et al. (2012), Variations in the abundances of potassium and thorium on the surface of Mercury: Results from the MESSENGER Gamma-Ray Spectrometer, *J. Geophys. Res.*, *117*, E00L04, doi:10.1029/2012JE004141.
Pettengill, G. H., and R. B. Dyce (1965), A radar determination of the rotation of the planet Mercury, *Nature*, *206*, 1240, doi:10.1038/2061240a0.
Phillips, R. J., et al. (2014), Mercury's 2nd-degree shape and geoid: Lunar comparisons and thermal anomalies, *Lunar Planet. Sci.*, *45*, Abstract 2634.
Redmond, H. L., and S. D. King (2007), Does mantle convection currently exist on Mercury?, *Phys. Earth Planet. Inter.*, *164*, 221–231, doi:10.1016/j.pepi.2007.07.004.
Rivoldini, A., and T. Van Hoolst (2013), The interior structure of Mercury constrained by the low-degree gravity field and the rotation of Mercury, *Earth Planet. Sci. Lett.*, *377*, 62–72, doi:10.1016/j.epsl.2013.07.021.
Schubert, G., D. L. Turcotte, and P. Olson (2001), *Mantle Convection in the Earth and Planets*, Cambridge Univ. Press, Cambridge, U. K., doi:10.1017/CBO9780511612879.
Smith, D. E., et al. (2012), Gravity field and internal structure of Mercury from MESSENGER, *Science*, *336*, 214–217, doi:10.1126/science.1218809.
Soter, S., and J. Ulrichs (1967), Rotation and heating of the planet Mercury, *Nature*, *214*, 1315–1316, doi:10.1038/2141315a0.
Stockstill-Cahill, K. R., T. J. McCoy, L. R. Nittler, S. Z. Weider, and S. A. Hauck II (2012), Magnesium-rich crustal compositions on Mercury: Implications for magmatism from petrologic modeling, *J. Geophys. Res.*, *117*, E00L15, doi:10.1029/2012JE004140.
Strom, R. G., N. J. Trask, and J. E. Guest (1975), Tectonism and volcanism on Mercury, *J. Geophys. Res.*, *80*, 2478–2507, doi:10.1029/JB080i017p02478.

Taylor, G. J., and E. R. D. Scott (2005), Mercury, in *Meteorites, Comets and Planets,* edited by A. M. Davis*, Treatise on Geochemistry,* vol. 1, edited by H. D. Holland and K. K. Turekian, pp. 477–485, Elsevier, Amsterdam, doi:10.1016/B0-08-043751-6/01071-9.

Tosi, N., M. Grott, A.-C. Plesa, and D. Breuer (2013), Thermochemical evolution of Mercury's interior, *J. Geophys. Res. Planets*, *118*, 2474–2487, doi:10.1002/jgre.20168.

Turcotte, D. L., and G. Schubert (2002), *Geodynamics*, 2nd ed., Cambridge Univ. Press, Cambridge, U. K., doi:10.2277/0521661862.

Turcotte, D. L., R. J. Willemann, W. F. Haxby, and J. Norberry (1981), Role of membrane stresses in the support of planetary topography, *J. Geophys. Res.*, *86*, 3951–3959, doi:10.1029/JB086iB05p03951.

Watters, T. R., R. A. Schultz, M. S. Robinson, and A. C. Cook (2002), The mechanical and thermal structure of Mercury's early lithosphere, *Geophys. Res. Lett.*, *29*, 1542, doi:10.1029/2001GL014308.

Weider, S. Z., L. R. Nittler, R. D. Starr, T. J. McCoy, K. R. Stockstill-Cahill, P. K. Byrne, B. W. Denevi, J. W. Head, and S. C. Solomon (2012), Chemical heterogeneity on Mercury's surface revealed by the MESSENGER X-Ray Spectrometer, *J. Geophys. Res.*, *117*, E00L05, doi:10.1029/2012JE004153.

Wessel, P., and W. H. F. Smith (1991), Free software helps map and display data, *Eos Trans. AGU*, *72*, 441–446, doi:10.1029/90EO00319.

Wieczorek, M. A. (2007), Gravity and topography of the terrestrial planets, in *Planets and Moons,* edited by T. Spohn*, Treatise on Geophysics,* vol. 10, edited by G. Schubert, pp. 165–206, Elsevier, Amsterdam.

Wieczorek, M. A. (2014), SHTOOLS – Tools for working with spherical harmonics (v2.9.1), Zenodo, doi:10.5281/zenodo.12158. [Available at https://zenodo.org/record/12158.]

Wieczorek, M. A. (2015), Gravity and topography of the terrestrial planets, in *Planets and Moons,* edited by T. Spohn*, Treatise on Geophysics,* vol. 10, 2nd ed., edited by G. Schubert, Elsevier, Amsterdam.

Wieczorek, M. A., and R. J. Phillips (1997), The structure and compensation of the lunar highland crust, *J. Geophys. Res.*, *102*, 10,933–10,944, doi:10.1029/97JE00666.

Wieczorek, M. A., and M. T. Zuber (2004), Thickness of the Martian crust: Improved constraints from geoid-to-topography ratios, *J. Geophys. Res.*, *109*, E01009, doi:10.1029/2003JE002153.

Wieczorek, M. A., et al. (2006), The constitution and structure of the lunar interior, *Rev. Mineral. Geochem.*, *60*, 221–364, doi:10.2138/rmg.2006.60.3.

Wieczorek, M. A., et al. (2013), The crust of the Moon as seen by GRAIL, *Science*, *339*, 671–675, doi:10.1126/science.1231530.

Zuber, M. T., et al. (2012), Topography of the northern hemisphere of Mercury from MESSENGER laser altimetry, *Science*, *336*, 217–220, doi:10.1126/science.1218805.